Journal of *Marine Science and Engineering*

MDPI

Article

Combined Longshore and Cross-Shore Modeling for Low-Energy Embayed Sandy Beaches

Yen Hai Tran [1,2,*], Patrick Marchesiello [3], Rafael Almar [3], Duc Tuan Ho [1,2,4], Thong Nguyen [1,2], Duong Hai Thuan [5] and Eric Barthélemy [6,*]

1 Faculty of Civil Engineering, Ho Chi Minh City University of Technology (HCMUT), 268 Ly Thuong Kiet Street, District 10, Ho Chi Minh City 700000, Vietnam; hotuanduc@hcmut.edu.vn (D.T.H.); nguyenthong@hcmut.edu.vn (T.N.)
2 Vietnam National University Ho Chi Minh City (VNU-HCM), Linh Trung Ward, Thu Duc District, Ho Chi Minh City 700000, Vietnam
3 Laboratoire d'Etudes en Géophysique et Océanographie Spatiales (LEGOS), Université de Toulouse/CNRS/CNES/IRD, 31400 Toulouse, France; patrick.marchesiello@ird.fr (P.M.); rafael.almar@ird.fr (R.A.)
4 Asian Centre for Water Research, Ho Chi Minh City University of Technology (HCMUT), 268 Ly Thuong Kiet Street, District 10, Ho Chi Minh City 700000, Vietnam
5 Faculty of Civil Engineering, Thuyloi University, Hanoi 116705, Vietnam; duonghaithuan@tlu.edu.vn
6 Laboratoire des Ecoulements Géophysiques et Industriels, Université Grenoble Alpes, CNRS, Grenoble-INP, 38000 Grenoble, France
* Correspondence: haiyen.tran@hcmut.edu.vn (Y.H.T.); Eric.Barthelemy@grenoble-inp.fr (E.B.)

Abstract: The present study focuses on the long-term multi-year evolution of the shoreline position of the Nha Trang sandy beach. To this end an empirical model which is a combination of longshore and cross-shore models, is used. The Nha Trang beach morphology is driven by a tropical wave climate dominated by seasonal variations and winter monsoon intra-seasonal pulses. The combined model accounts for seasonal shoreline evolution, which is primarily attributed to cross-shore dynamics but fails to represent accretion that occurs during the height of summer under low energy conditions. The reason is in the single equilibrium Dean number Ω_{eq} of the ShoreFor model, one of the components of the combined model. This equilibrium Dean number cannot simultaneously account for the evolution of strong intra-seasonal events (i.e., winter monsoon pulses) and the annual recovery mechanisms associated with swash transport. By assigning a constant value to Ω_{eq}, when the surf similarity parameter is higher than 3.3 (occurrence of small surging breakers in summer), we strongly improve the shoreline position prediction. This clearly points to the relevance of a multi-scale approach, although our modified Ω_{eq} retains the advantage of simplicity.

Keywords: shoreline model; one-line model; embayed beach; low-energy beach; cross-shore; longshore

Citation: Tran, Y.H.; Marchesiello, P.; Almar, R.; Ho, D.T.; Nguyen, T.; Thuan, D.H.; Barthélemy, E. Combined Longshore and Cross-Shore Modeling for Low-Energy Embayed Sandy Beaches. *J. Mar. Sci. Eng.* **2021**, *9*, 979. https://doi.org/10.3390/jmse9090979

Academic Editor: Celene B. Milanes

Received: 12 August 2021
Accepted: 2 September 2021
Published: 7 September 2021

1. Introduction

Empirical data-driven models are increasingly being used for modeling shoreline changes on time scales from days to decades [1–9]. They are based on a set of parameters representing the contribution of complex physical processes that are evaluated on a calibration period using observed shoreline data. These models are simpler but also much less computationally expensive to simulate long-term shoreline changes than physics-based models such as Delft3D [10], XBeach [11], or Mike21 [12]. These data-driven empirical models essentially apply to natural beaches with no anthropic interference, beaches that are more or less in equilibrium with the wave forcing conditions.

On one hand, shoreline changes on small time scales for such type of beaches are primarily attributed to cross-shore transport [7]. The cross-shore empirical models used for long-term predictions predominantly assume that a sandy beach tends towards an

equilibrium for a wave forcing uniform in time [5,13,14]. The shoreline evolution can thus be represented as a relaxation process towards equilibrium [15,16] that takes the form

$$\frac{\partial S}{\partial t} = F(\Delta\Omega) \tag{1}$$

where $S(t)$ is the shoreline position in the transect; t is time; $\frac{\partial S}{\partial t}$ is the rate of shoreline change; Ω is the dimensionless fall velocity (Dean number or Gourlay number): $\Omega = \frac{H}{w_s T}$, a function of H the offshore significant wave height, w_s the sediment fall velocity, and T the peak wave period; and $\Delta\Omega$ is called the disequilibrium Dean number, $\Delta\Omega = \Omega_{eq} - \Omega$, where Ω_{eq} represents the equilibrium forcing. The success of cross-shore models relies on the timescale used to correct the disequilibrium of shoreline position under a particular forcing. To improve its predictive skills, the work in [17] uses a multi-timescale approach, which accounts for storms and seasonal and inter-annual wave climate variability, including the scale interactions between these different forcings.

On the other hand, long-term evolution is generally associated with the longshore drift, i.e., the transport of sediments by wave-driven currents along the coast. In one-line models, the littoral drift is the only mechanism of shoreline evolution. The theory in [18] is regarded as a cornerstone of these models, which describes the shoreline evolution due to beach curvature $\frac{\partial^2 S}{\partial x^2}$, following a diffusion equation (with κ a diffusion coefficient):

$$\frac{\partial S}{\partial t} = \kappa \frac{\partial^2 S}{\partial x^2} \tag{2}$$

Longshore transport can be significant even on a seasonal scale on very curved coastlines such as embayed beaches [19]. These shorelines may rotate in time around a pivotal point due to changing wave directions. To translate a longshore drift gradient into a change in the shoreline, it is assumed in one-line models that the beach profile moves in a direction transverse to the coast while maintaining its unchanging shape [2]. A second assumption is that sand is transported alongshore between the active berm and a closure depth h_c, beyond which the beach is inactive, i.e., there is no erosion or accretion [20]. In this case, the shoreline changes with the alongshore gradient of the volumetric longshore transport rate Q_x as

$$\frac{\partial S}{\partial t} = -\frac{1}{h_c + B} \frac{\partial Q_x}{\partial x} \tag{3}$$

where B is the berm height, and Q_x is a function of the breaking wave height and longshore direction, i.e., the longshore wave power, as in the widely used CERC formula [21]. There are a number of such models based on various additional features and numerical implementations [22–25]. A wave sheltering procedure for large wave angles, which triggers an instability mechanism generating large-scale morphology over long timescales, is introduced by [22]. A new vector-based model with more flexible shoreline cell shape is suggested by [23]. The GSb model [9,25] is based on the one-line approach to investigate the longshore drift at a coastal mound made up of non-cohesive sediments, e.g., sand, gravel, cobbles, shingle, and rock. The ShorelineS model in [24] is the latest model for long-term shoreline evolution and is capable of simulating rich coastal transformation behavior of complex shoreline features through its flexible grid.

For a coastline dominated by both cross-shore and longshore transport, as for embayed beaches, a model that considers both transport processes is expected to improve a skillful hindcast. An integrated shoreline model considering sea-level rise in addition to cross-shore and longshore transport is developed in [6] . In this model, called CosMos-COAST, the cross-shore contribution to shoreline change is based on the work in [13], the longshore contribution is based on the one-line concept in [18], and the last contribution is from the sea level rise response model in [26]. Other combinations such as that of [7] who combine the ShoreFor cross-shore model in [5] and a hybrid one-line approach derived in [22]. Along this line [1] suggested coupling the ShoreFor model with a simpler longshore

model based on a sediment budget and the empirical CERC formula [21]. In the latter, it is assumed that an equilibrium exists in the form of an average shoreline position. Thus, the longshore model variables can be decomposed into a mean and fluctuating contribution in the time series.

In the present study, we will pay particular attention to the suitability of a longshore model for embayed beaches and the ability of a single equilibrum cross-shore model to represent accretion during summer low wave energy conditions. Nha Trang, Vietnam, is an embayed beach with a curved shoreline [27], and thus provides a good test case for the combined model of [1] that accounts for both cross-shore and longshore contributions. Nha Trang's climate is characterized by strong seasonal forcing, i.e., summer monsoons with low-energy waves and winter monsoons with high-energy waves, including intra-seasonal winter pulses [28,29]. Because shoreline evolution models are typically calibrated with data from moderate- to high-energy beaches [5,6], the case of low-energy beaches was neglected, even though, as we will see, they present an additional challenge to these models.

In Section 2, the combined model of the work in [1] is briefly recalled. Section 3 describes the characteristics of Nha Trang beach. The result of the combined model implemented on the embayed beach shoreline of Nha Trang is presented in Section 4, and Section 5 presents the concluding remarks.

2. Methods

The combined model of Tran and Barthélemy (2020) [1] is built by replacing in the ShoreFor model equation of the work in [5] the free parameter d (representing a long-term trend) with a longshore model equation. The combined model is written as

$$\frac{\partial S}{\partial t} = c\left(F^{+} + rF^{-}\right) + H_b^{3/2}\left[a\cos 2\alpha_b{}' + b\sin 2\alpha_b{}'\right] \tag{4}$$

where t is time in days; $S(t)$ is the shoreline position; and F^{+} and F^{-} represent the accretion and erosion forcing terms, respectively [5]. The parameter r is called the erosion ratio [5]. The forcing term F is the product of the incident wave power P and the disequilibrium Dean number $\Delta\Omega$ [5]. $\Delta\Omega$ is defined by $\Delta\Omega(t) = \Omega(t) - \Omega_{eq}(t)$. $\Omega(t)$ is the instantaneous Dean number. $\Omega_{eq}(t)$ is the equilibrium Dean number which is defined by [14,16]

$$\Omega_{eq}(t) = \frac{\sum_{j=1}^{\frac{2\phi}{\Delta t}} \Omega_j 10^{-j\Delta t/\phi}}{\sum_{j=1}^{\frac{2\phi}{\Delta t}} 10^{-j\Delta t/\phi}} \tag{5}$$

where ϕ (day) is the "memory decay", Δt is the wave forcing data time step, and j is the number of data points in the survey time series prior to the calculation point at time t [14].

In Equation (4), a, b, and c ($m^{1.5} days^{-1} W^{-0.5}$) are free parameters obtained from optimization. H_b is the significant wave height at breaking point. α_b' is the fluctuation of the orientation of the incident wave field, $\alpha_b' = \alpha_b - \overline{\alpha_b}$; α_b is the orientation angle of the incident wave field (Figure 1) and $\overline{\alpha_b}$ is the average. Figure 1 shows a plan view of the incident wave orientation angle α and the beach orientation angle β. In the longshore model, the equilibrium shoreline orientation $\overline{\beta}$ and the average breaking wave propagation direction $\overline{\alpha_b}$ need to meet the condition [1]

$$\overline{\beta}(x) = \overline{\alpha_b}(x) + \frac{1}{2}\psi(x) \tag{6}$$

where ψ is defined by $\tan\psi \simeq \frac{\overline{H^{5/2}\sin 2\alpha_b'}}{\overline{H^{5/2}\cos 2\alpha_b'}}$. ψ depends on correlations between the wave height and the wave direction. If the value of ψ is small, $\overline{\beta}$ approximates $\overline{\alpha_b}$. The average incident wave direction is thus perpendicular to the shoreline. On a scale of several years, the embayed beach is assumed to be balanced if the wave direction is invariable and orthogonal to the shoreline.

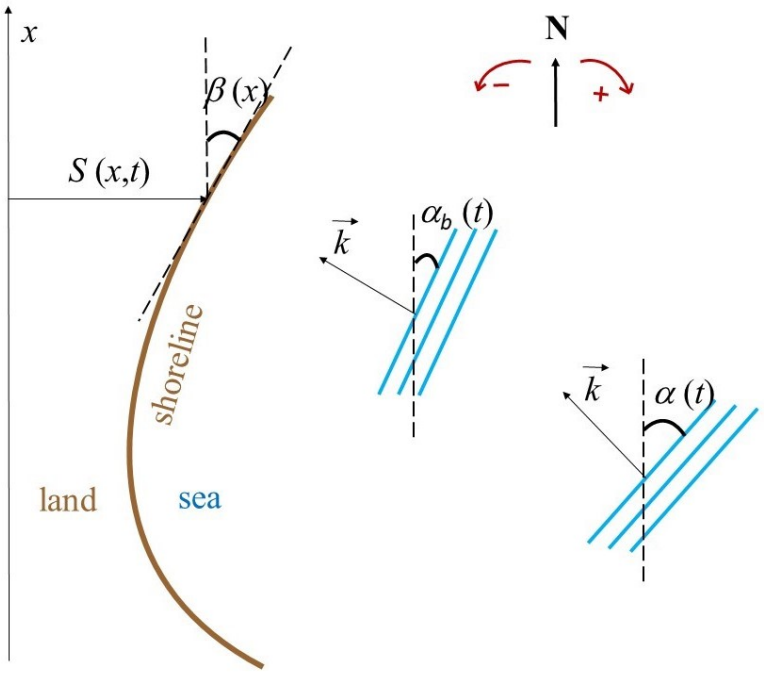

Figure 1. Plan view of the incident wave orientation angle α and the beach orientation angle β. From the vertical line, an angle measured clockwise is positive and an angle measured counterclockwise is negative. α_b denotes the breaking wave angle. S denotes the shoreline position with respect to an arbitrary vertical baseline. $\vec{k}$ is the wave vector. N stands for the north.

In fact, there are four free parameters to drive the model: a, b, c, and ϕ. The free parameters will be obtained from the Simulated Annealing optimization method [30] to minimize the root mean square error (RMSE) between the observed and modeled shoreline data [4].

3. Study Site

3.1. Site Description

Nha Trang beach is a 6 km-long embayed beach, located on the southeastern Vietnam coast (Figure 2). The Cai River estuary borders on the beach in the north. The beach is sheltered by Hon Tre, Hon Tam, and Hon Mieu islands in the south. The tide regime is microtidal and a mix of diurnal and semidiurnal with a tidal range of roughly 1.5 m at spring tide. The beach is classified as a flat low-tide terrace and a steep beach face slope (≈0.1) [29]. The mean sand grain size is 0.4 mm. The survey transect considered in this study is at the field experiment location of the project of Coastal Variability in West Africa and Vietnam (COASTVAR) in the north of Nha Trang beach (Figure 3) [29].

3.2. Waves

The beach of Nha Trang is sheltered and the waves are generally of lower energy than on the open coast [27–29]. Waves are affected by summer monsoons from May to September and winter monsoons from October to April (Figure 2). Local islands shelter the bay from waves induced by southwest summer monsoons (Figure 2). Northeast winter monsoons drive stronger waves locally. From August to December, typhoons approach Nha Trang typically from the NE direction. It is noteworthy that during the calibration period, 2013–2016, two extremely strong typhoons entered Nha Trang, namely, Nari and Haiyan, on 15 October and 10 November 2013, respectively.

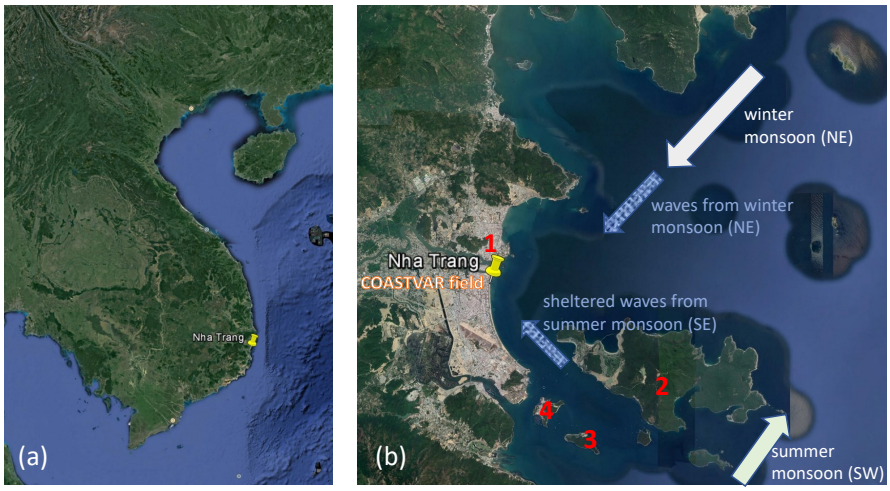

Figure 2. (**a**) Location of Nha Trang beach on Vietnam map. (**b**) Nha Trang bay with Cai River estuary (1) in the north and a group of islands in the south, e.g., Hon Tre (2), Hon Tam (3), and Hon Mieu (4).

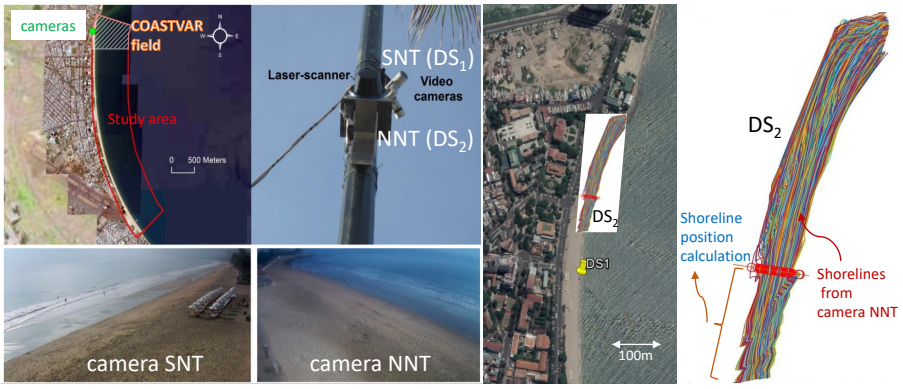

Figure 3. Area of interest (COASTVAR field experiment location) with the location of video cameras and shoreline detection by video imagery.

4. Application, Result and Discussion

4.1. Shoreline Data

Two shoreline datasets obtained from video imagery of two cameras are used to calibrate the shoreline model [27]. For each day in the time-series, the shoreline is identified from video images at a time corresponding to the same tidal level, i.e., the mean tidal level of the calibration period [29,31]. Figure 3 shows the location and snapshot of the video cameras installed from May 2013: one camera facing south (camera SNT) and one facing north (camera NNT). Shoreline dataset 1 (DS_1) is from the camera SNT and shoreline dataset 2 (DS_2) is from the camera NNT. DS_1 was obtained from time-stack video images of a single cross-shore section (Figure 3) at the COASTVAR experiment location [29,32,33]. These data represent the daily shoreline change for a full year, from July 2013 to August 2014 [29]. DS_2 from the NNT video camera was collected during 2.5 years from May 2013 to December 2015 [31]. The shoreline in DS_2 was detected for a distance of 300 m along the coast, north of DS_1 (Figure 3). In this study, the shoreline position of DS_2 was calculated by taking the average along the coast of about 100 m in the southern part of the entire detection region, which is close to DS_1 (Figure 3). The shoreline position data of the two datasets are plotted in Figure 4. The mean time interval of the shoreline data is 1 day.

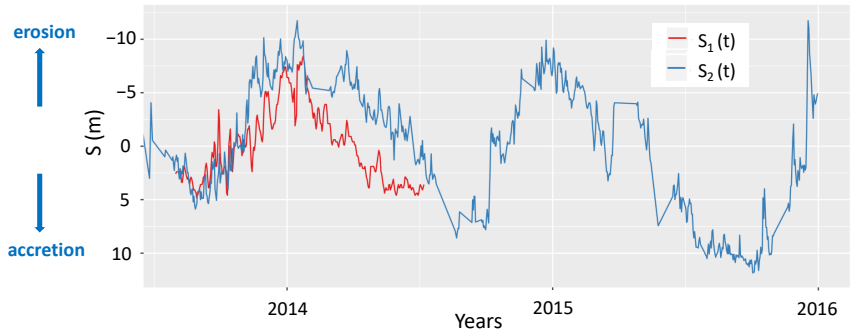

Figure 4. Time series of shoreline position $S_1(t)$ from DS_1 (red line) and $S_2(t)$ from DS_2 (blue line).

4.2. Wave Input Data

The 6 h interval ERA-Interim offshore wave data from the European Center for Medium-Range Weather Forecasts (ECMWF) from May 2013 to December 2015 are propagated and transformed by the Simulating WAves Nearshore model (SWAN) up to 10 m water depth and at breaking point [34]. SWAN is a third-generation wave model for obtaining realistic estimates of wave parameters in coastal areas, lakes, and estuaries from given wind, bottom, and current conditions [35]. The bathymetry data input in SWAN is a combination of data of the General Bathymetric Chart of the Oceans (GEBCO) and COASTVAR measured topography data (Figure 5). The resolution of GEBCO data is approximately 800 m. The COASTVAR measured topography data are very detailed in the near-shore zone. The wave data results at 10 m depth and at breaking point are used for shoreline evolution modeling. The time interval of the wave fields including H_s, T_p, and α is 1 h. Locations of the point at 10 m depth and of breaker line used for extracting SWAN wave outputs are shown in Figure 6a. They are near to the COASTVAR shoreline detection location. The breaking wave is defined indirectly from the significant wave height and the water depth extracted from SWAN outputs to calculate the breaking index γ [7,36]. γ is the ratio of the wave height to the water depth. The criterion for wave breaking is taken when γ is about 0.78. The SWAN computational grid of 20 m is too large to define the locations where γ is 0.78. A region of 400 m$\times$ 400 m near the beach including the surf zone is thus extracted from the computational grid to find the grid cells having γ in the range from 0.4 to 0.8 [34]. Figure 6a,b shows the region of 400 m $\times$ 400 m extracted for the breaker line determination. It is clear that the range from 0.4 to 0.8 of the breaking index provides the breaker line which is continuous along the shoreline and parallel to the shoreline (Figure 6a). The significant wave height and the wave direction at breaking point are calculated by taking mean value at these grid points. Figure 6c,d shows the wave roses at 10 m water depth and at breaking point, respectively. Figure 7a shows the time series of the significant wave height H_s at 10 m depth. It ranges from 0.01 m to 1.71 m and the mean value is 0.43 m. It is noticed that the significant wave height in summer has very small values corresponding with the large values of the surf similarity parameter (Figure 7b). The surf similarity parameter [37] or the Iribarren number ξ is used to classify breaker types, given by

$$\xi = \frac{m}{\sqrt{H_\infty / L_\infty}} \tag{7}$$

where m is the beach slope, H_∞ is the deep-water wave height, and L_∞ is the deep-water wave length. The surf similarity parameter ξ represents the influence of the beach slope on the wave geometry. There are three main types of breaking, such as spilling ($\xi < 0.5$), plunging ($0.5 < \xi < 3.3$), and surging ($\xi > 3.3$) [38]. Figure 7b shows the time series of the surf similarity parameter ξ. In this case, the wave parameters at 10 m depth were used to calculate ξ.

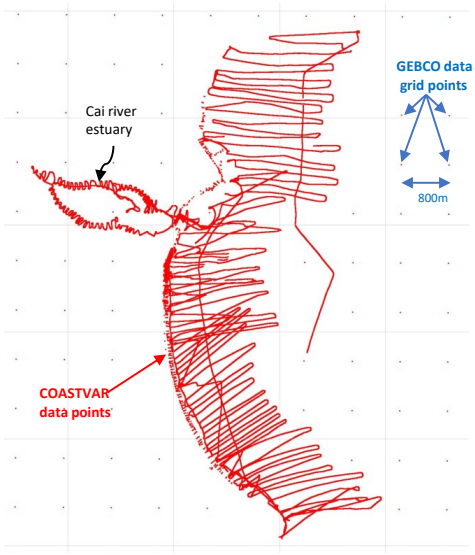

Figure 5. Bathymetry data input includes GEBCO data grid points and COASTVAR measured topography data points.

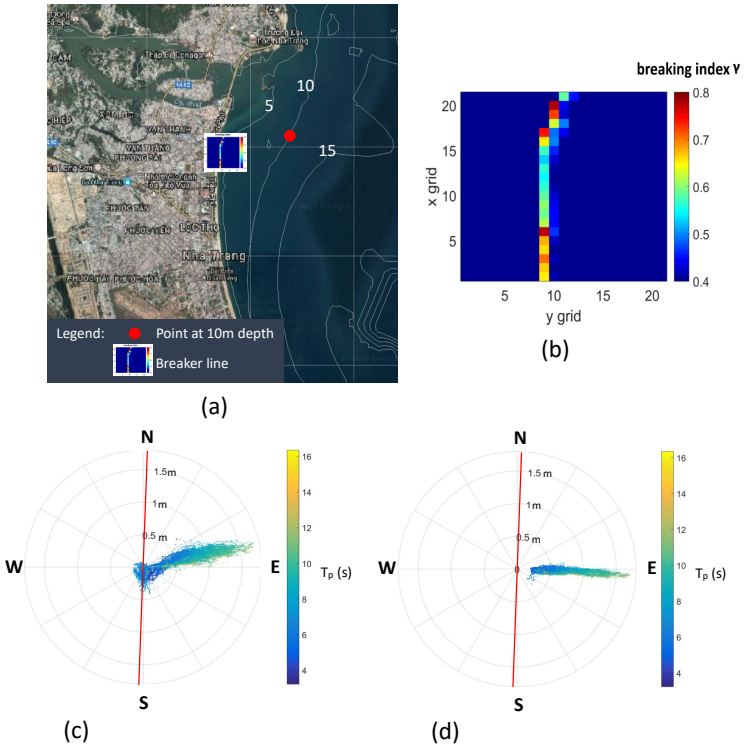

Figure 6. (**a**) Locations of point at 10 m depth and of breaker line used for extracting SWAN wave characteristics. (**b**) Breaker line along the shoreline at PF1 detected from a SWAN grid region of 400 m × 400 m; colorbar indicates the breaking index. "x grid" is the index of "X", while "y grid" is the index of "Y"; "pixel" is a grid cell of 20 m × 20 m. Directional plot of the significant wave height H_s (circles) and the peak wave period T_p (colorbar) from SWAN at 10 m water depth (**c**) and at breaking point (**d**). The red line is the beach orientation. North (N) corresponds to 0°.

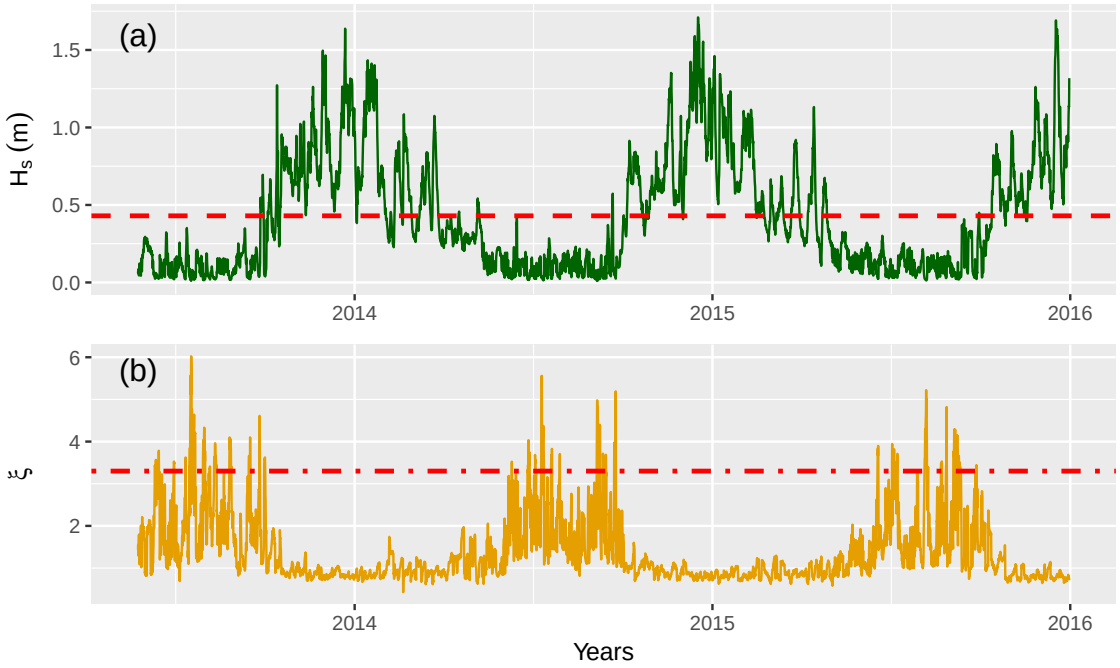

Figure 7. (**a**) Time series of SWAN significant wave height H_s at 10 m depth (green line) and the horizontal line at its mean value = 0.43 m (red dashed line). (**b**) Time series of the surf similarity parameter ξ (yellow line) and the horizontal line at the threshold value of $\xi = 3.3$ (red dashed line).

4.3. Result

The equilibrium shoreline orientation in Equation (6) is first verified before calibrating the combined model. Both the wave data at breaking point and at 10 m depth are used for the equilibrium condition verification for each of the five transects defined in Figure 8 (Table 1). Along the shoreline, we have selected 5 transects: PF1, PF2, PF3, PF4, and PF5 (Figure 8). The transect PF1 is at the COASTVAR field experiment location.

Figure 8. The five profile transects of interest. S_0m is considered the landmark position.

Table 1. Values of ψ_b, ψ_{10}, $\overline{\alpha_b}$, $\overline{\alpha_{10}}$, $\overline{\beta_b}$, $\overline{\beta_{10}}$, and β_m. β_m is the beach orientation measured on Google Earth images.

Transect	ψ_b	ψ_{10}	$\overline{\alpha_b}$	$\overline{\alpha_{10}}$	$\overline{\beta_b}$	$\overline{\beta_{10}}$	β_m
PF1	−0.27°	−58.53°	2.68°	18.02°	2.54°	−11.25°	2°
PF2	−0.53°	−56.88°	−5.12°	12.87°	−5.38°	−15.57°	−1°
PF3	−0.99°	−59.06°	−13.58°	4.60°	−14.08°	−24.93°	−10°
PF4	−1.38°	−60.02°	−25.77°	−4.99°	−26.46°	−35°	−22°
PF5	−4.58°	−70.16°	−39.38°	−14.87°	−41.67°	−49.95°	−36°

β_m is the average of the beach orientation measured in time on Google Earth images during the calibration period. Table 1 shows that β_b is a closer guess to β_m than β_{10} which gives confidence in the SWAN simulations. The results indicate that ψ_b has a small contribution to the beach orientation. The assumption on the angles used in Equation (6) is thus validated. The wave data at breaking point will thus be used for the longshore component of the combined model. The cross-shore component of the combined model (4) is calibrated with the SWAN wave data at 10 m depth (Figure 9a).

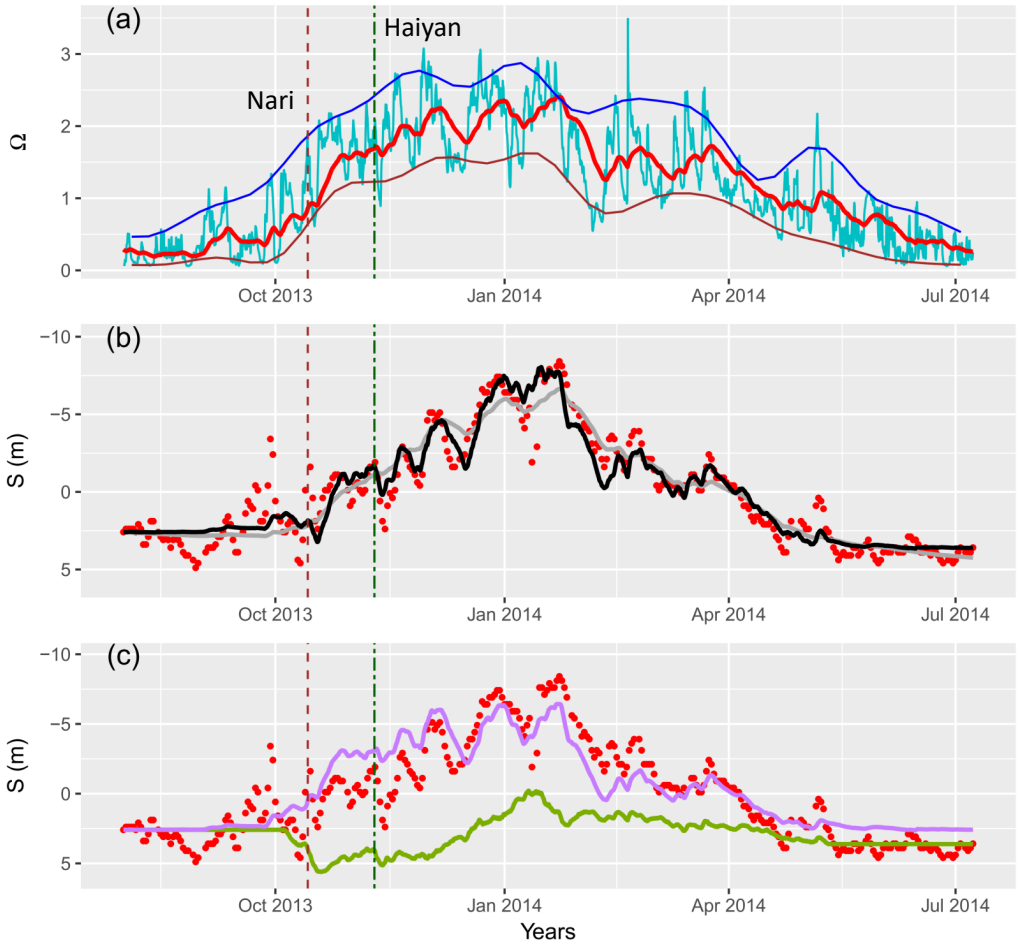

Figure 9. The combined model calibrated with DS_1. (**a**) Time series of Ω (green line), Ω_{eq} (red line), upper envelope (blue line) and lower envelope (brown line), vertical lines indicate the time of Nari and Haiyan typhoons. (**b**) Time series of measured shoreline position (red points); shoreline position from combined model (black line); shoreline position from ShoreFor model (gray line). (**c**) Cross-shore contribution (purple line) and longshore contribution (green line).

The combined model calibrated with DS_1 gives the smallest RMSE of 1.12 m for $\phi = 20$ days (Figure 9b). The parameters a, b, c, and r are 0.0251, 4.9432, 0.0146, and 0.4702, respectively. The optimal value of $\phi = 20$ days for the combined model is small in comparison with 70 days found with the ShoreFor model alone. It indicates that the longshore component interacts with the cross-shore equilibrium state. With the longshore contribution, the equilibrium Dean numbers are computed with a smaller memory decay ϕ, i.e., the modeled beach state reaches equilibrium on shorter time scales. Figure 9c shows a clear seasonal shoreline change of the longshore contribution at the Nha Trang beach. From November to January in winter monsoons, it has an eroding trend with an amplitude of 5 m, and from February to May in summer monsoons, it has an accreting trend with an amplitude of 3.5 m. In the middle of October 2013 and early November 2013, the longshore contribution gives a small accretion trend even though Nari and Haiyan typhoons hit the coast (Figure 9c). The measured shoreline position indicates that these two typhoons have driven strong erosion events, and then the beach has had a fast recovery immediately after that [29,31]. In fact, during the COASTVAR campaign, it was observed that a storm event hit the coast and caused erosion but then the beach also quickly recovered [32,33,39,40]. It appears that the longshore contribution of the model tends to favor accretion/recovery immediately after the storm (Figure 9c).

The combined model is also calibrated with DS_2 which is longer than DS_1 (Figure 10). This time, the smallest RMSE is 3.27 m for $\phi = 70$ days. The three calibration-free parameters—a, b, and c—are 0.0081, 1.1548, and 0.0113, respectively. The erosion ratio r is 0.2358. From Figure 10a, the upper and lower envelopes of Ω clearly show yearly cycles. Waves in Nha Trang are strongly affected by the tropical climate with two distinct seasons: small waves with small Ω in summer and strong waves with strong Ω in winter. Ω_{eq} has a variability time scale of one year just as the forcing Ω. Figure 10a also shows how ϕ affects the equilibrium Dean number Ω_{eq} computations. In the first part of winter, as the envelope increases, the equilibrium Dean number Ω_{eq} is less than the instantaneous Dean number Ω, so the model gives a strong erosion (Figure 10b). Because $\phi = 70$ days, Ω_{eq} is affected by the small values of Ω from the summer period. This ϕ value thus produces a strong phase shift of Ω_{eq}. In the next phase, as Ω_{eq} becomes larger than Ω, the model gives an accretion (Figure 10b). Figure 10b shows that the modeled shoreline position reproduces the observed annual cycle of erosion and accretion, although there are large discrepancies during the accretion phase. Figure 10c shows that only a small part of the seasonal shoreline change is described by the longshore contribution while the synoptic to seasonal time scales of shoreline change are mainly due to the cross-shore contribution.

4.4. Discussion

The most striking result of the model is that the accretion sequence is poorly reproduced during the summer monsoons (Figure 10b). This is due to the memory decay used in the weighted averaging for Ω_{eq} in Equation (5). During summer monsoons, the small wave forcing leads to a small Ω_{eq}, very similar to the instantaneous Dean number Ω, so that the disequilibrium Dean number is small and induces a small shoreline variation. This suggests that an intra-seasonal memory decay is not appropriate for summer conditions and a multi-scale approach should be considered [17,41]. Alternatively, here, the definition of Ω_{eq} is re-valuated for summer.

During much of summer monsoons, the surf similarity parameter ξ is higher than 3.3 (Figure 7b). The breaking waves can be thus classified as surging breakers, and nearshore waves may not even break at all. The shoreline measurements indicate that there are no breaking waves, so the longshore contribution is zero, but small waves on a long period still contribute to cross-shore accretion. The surging breakers induce strong swash and gentle backwash that produces shoreward sand transport [42]. As a result, the shoreline tends to accrete in summer.

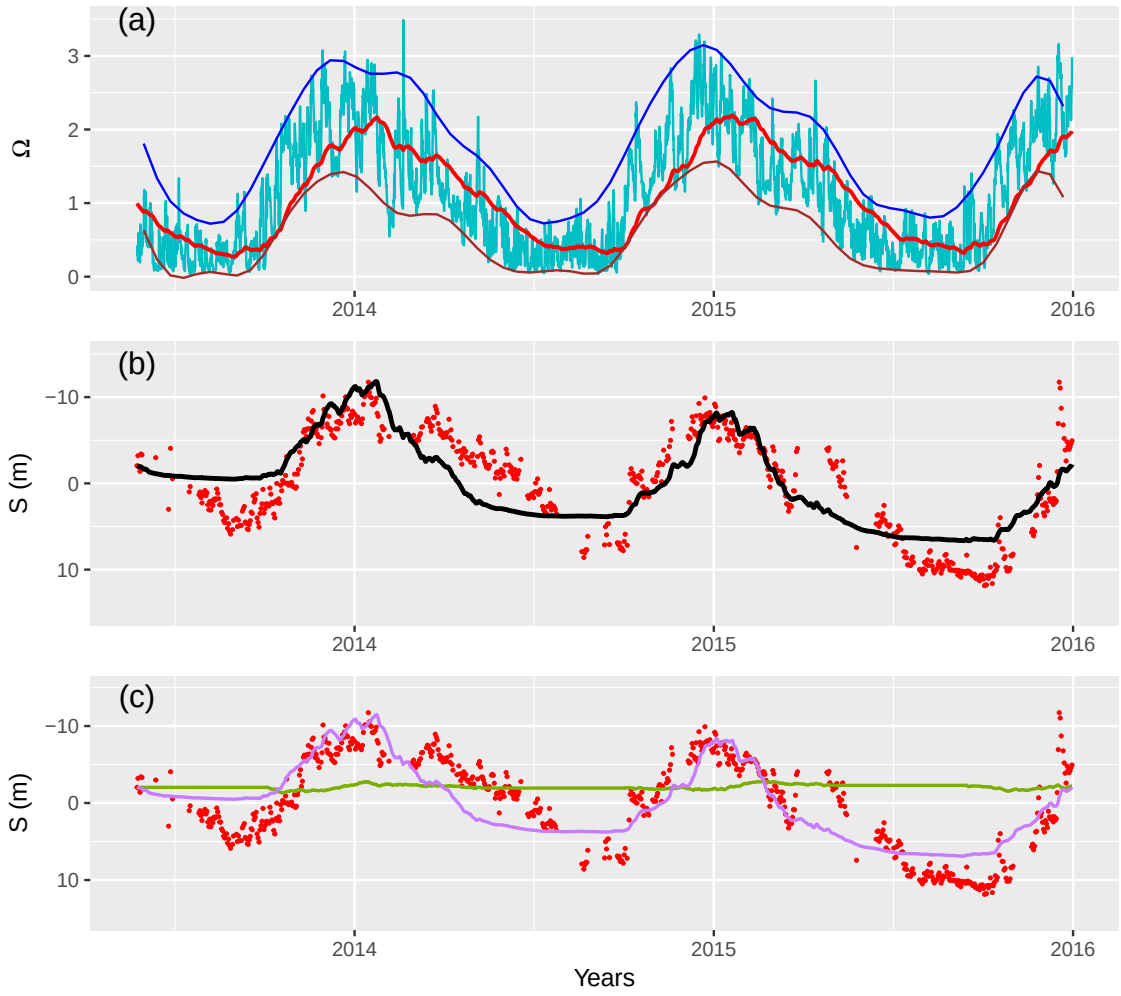

Figure 10. The combined model calibrated with DS_2. (**a**) Time series of Ω (green line), Ω_{eq} (red line), upper envelope (blue line), lower envelope (brown line) and inter-annual average (black line), (**b**) Time series of measured shoreline position (red points) and shoreline position from combined model (black line), (**c**) Cross-shore contribution (purple line), longshore contribution (green line).

In the original ShoreFor formulation [14], the equilibrium forcing Ω_{eq} was constant and represented an annual value. This formulation was more favorable to seasonal variations. In our case, Ω would be lower than Ω_{eq} at the peak of summer and accretion would continue until the onset of winter monsoon. However, for Ω_{eq} varying at intra-seasonal scale (to deal with winter monsoon pulses), the model looses its relaxation mechanism at the annual scale, which is associated with swash processes and summer accretion.

To remedy to this summer limitation, we consider the special case of very low energy waves with surf similarity parameter ξ higher than 3.3. In this case, Ω_{eq} is assigned a constant value of 0.8 (near the annual mean), so that the beach would accrete in summer when $\Omega(t) < 0.8$ and $\xi > 3.3$ (Figure 11a). Figure 11b confirms that the shoreline position from the combined model with modified Ω_{eq} improves significantly and the modeled shoreline position is now remarkably close to observations during the summer (compare Figure 11b with Figure 10b). The RMSE is 2.25 m, which is much lower than the previous one (3.27 m). The values of the calibration parameters a, b, and c are 0.0239, 3.015, and 0.0195, respectively. The erosion ratio r is 0.5413, and the optimal memory decay ϕ is now 20 days instead of 70 days in the previous case. The relatively short time scale of 20 days encompasses that of winter monsoon pulses [28], on which the model can now focus more optimally. This is in line with the multi-scale approach of ShoreFor developed in [17,41], but within a simpler formulation. Figure 11c also shows that the seasonal fluctuation of the longshore

contribution is now more pronounced than in the previous calibration (Figure 10c). For a longer interannual evolution, a period of three years is still too short and we will rely in the future on satellite monitoring for periods up to 30 years [43–45]. This will likely help in understanding the interaction between wave forcing and shoreline evolution at different time scales.

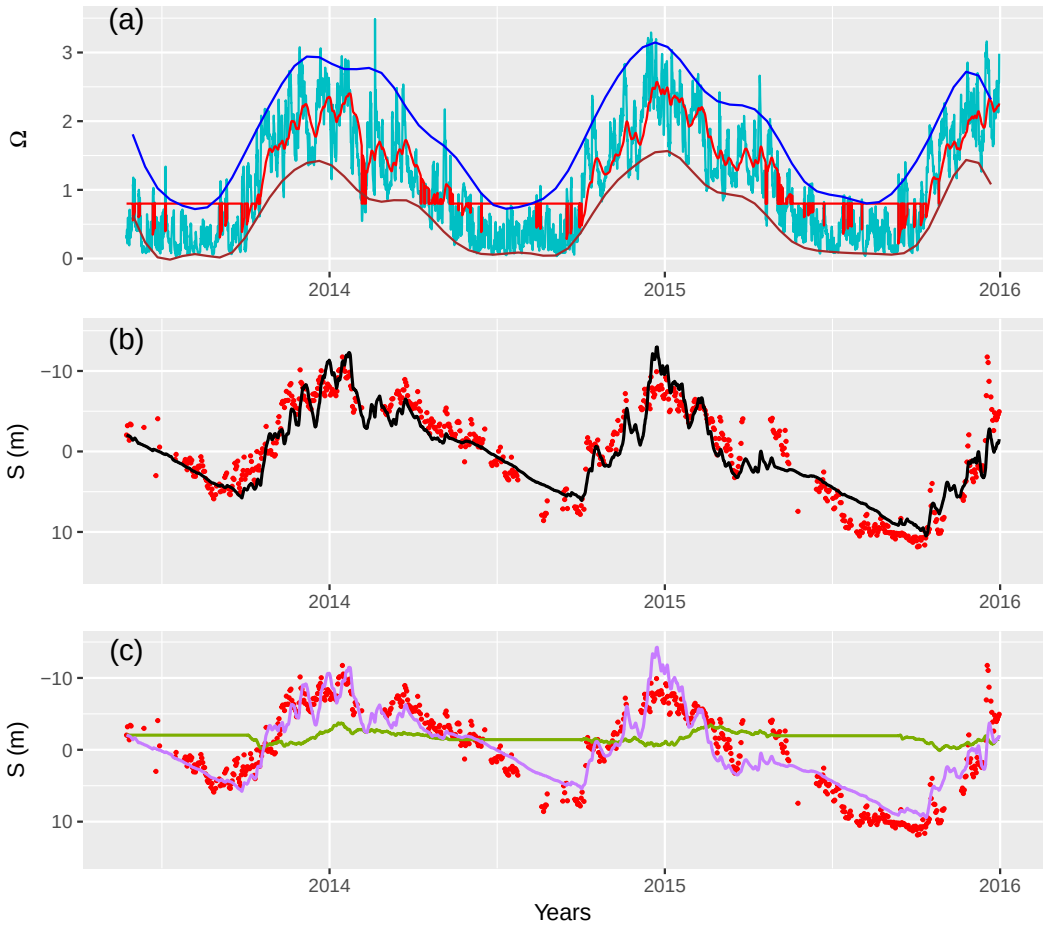

Figure 11. The combined model calibrated with DS_2 and modified equilibrium Dean number in summer. (**a**) Time series of Ω (light-blue line), Ω_{eq} (red line), upper envelope (blue line), lower envelope (brown line). (**b**) Time series of measured shoreline position (red points) and modeled shoreline position (black line). (**c**) Time series of the longshore contribution (green line) and the cross-shore contribution (purple line).

5. Conclusions

The results from the combined model calibrated with Nha Trang shoreline data and SWAN wave fields are an improvement over those of the ShoreFor model. The longshore contribution slightly improves the variability of the modeled shoreline position, especially with the shoreline data DS_1. Interestingly, the seasonal cycle of the coastline is weakly affected by the longshore contribution and is better explained by the cross-shore transport.

In addition, we suggest that the definition of the equilibrium Dean number should be modified for very low-energy waves ($\xi > 3.3$), in summer, under conditions without intra-seasonal wave events. It is a way to resolve contrasting behaviors at multiple scales. Without this modification, it is difficult to find an optimal memory parameter ϕ that represents in the same time the action of high-energy winter monsoon events at scales of 3–20 days and annual recovery mechanisms associated with swash transport. By assigning an annual mean value to the equilibrium Dean number Ω_{eq} when the surf similarity ξ_0 is higher than 3.3, we obtain a much smaller error of shoreline position. This enhancement simply mimics the slow but long process of shoreline accretion under very light waves.

Although the combined model provides better predictive capabilities than the cross-shore model alone, the latter remains the main source of uncertainty at small time scales (<decades). A large part of the uncertainty appears related to the way Ω_{eq} is defined. Our results clearly points to the relevance of a multi-scale approach in this regard, although our modified formulation keeps the advantage of simplicity.

Author Contributions: Conceptualization, E.B.; methodology: E.B., T.N., D.T.H.; software, Y.H.T.; validation, E.B., P.M., R.A. and Y.H.T.; data curation, R.A., D.H.T. and Y.H.T.; writing—original draft preparation, Y.H.T.; writing—review and editing, E.B., P.M., R.A. and Y.H.T.; visualization, Y.H.T.; funding acquisition, D.T.H. and T.N. All authors have read and agreed to the published version of the manuscript.

Funding: This research is funded by Ho Chi Minh City University of Technology (HCMUT), VNU-HCM under grant number Tc-KTXD-2020-01.

Institutional Review Board Statement: Not applicable.

Informed Consent Statement: Not applicable.

Data Availability Statement: The data that support the findings of this study are available from the corresponding author, [R.A. and D.H.T.], upon reasonable request.

Acknowledgments: This research has been conducted under the framework of CARE-Rescif initiative and the Ho Chi Minh City University of Technology (HCMUT), VNU-HCM under grant number Tc-KTXD-2020-01. We acknowledge the support of time and facilities from HCMUT, VNU-HCM, LEGI-INPG, CARE-Rescif for this study. Y.H.T. was funded by the French Embassy in Hanoi for the PhD grant "Bourse d'Excellence".

Conflicts of Interest: The authors declare no conflict of interest.

Abbreviations

The following abbreviations are used in this manuscript:

COASTVAR	Coastal Variability in West Africa and Vietnam
CosMos-COAST	Coastal One-line Assimilated Simulation Tool
ECMWF	European Center for Medium-Range Weather Forecasts
GEBCO	General Bathymetric Chart of the Oceans
RMSE	root mean square error
SWAN	Simulating WAves Nearshore model

References

1. Tran, Y.H.; Barthélemy, E. Combined longshore and cross-shore shoreline model for closed embayed beaches. *Coast. Eng.* **2020**, *158*, 103692. [CrossRef]
2. Hanson, H.; Kraus, N.C. *GENESIS: Generalized Model for Simulating Shoreline Change. Report 1. Technical Reference*; Coastal Engineering Research Center: Vicksburg, MS, USA, 1989.
3. Davidson, M.A.; Turner, I.L. A behavioral template beach profile model for predicting seasonal to interannual shoreline evolution. *J. Geophys. Res. Earth Surf.* **2009**, *114*. [CrossRef]
4. Castelle, B.; Marieu, V.; Bujan, S.; Ferreira, S.; Parisot, J.; Capo, S.; Sénéchal, N.; Chouzenoux, T. Equilibrium shoreline modelling of a high-energy mesomacrotidal multiple-barred beach. *Mar. Geol.* **2014**, *347*, 85–94. [CrossRef]
5. Splinter, K.D.; Turner, I.L.; Davidson, M.A.; Barnard, P.; Castelle, B.; Oltman-Shay, J. A generalized equilibrium model for predicting daily to interannual shoreline response. *J. Geophys. Res. Earth Surf.* **2014**, *119*, 1936–1958. [CrossRef]
6. Vitousek, S.; Barnard, P.L.; Limber, P.; Erikson, L.; Cole, B. A model integrating longshore and cross-shore processes for predicting long-term shoreline response to climate change. *J. Geophys. Res. Earth Surf.* **2017**, *122*, 782–806. [CrossRef]
7. Robinet, A.; Idier, D.; Castelle, B.; Marieu, V. On a reduced-complexity shoreline change model combining longshore and cross-shore processes: The LX-Shore model. *Environ. Model. Softw.* **2018**, *109*, 1–16. [CrossRef]
8. Montaño, J.; Coco, G.; Antolínez, J.A.; Beuzen, T.; Bryan, K.R.; Cagigal, L.; Castelle, B.; Davidson, M.A.; Goldstein, E.B.; Vos, K.; et al. Blind testing of shoreline evolution models. *Sci. Rep.* **2020**, *10*, 2137. [CrossRef] [PubMed]
9. Tomasicchio, G.R.; Francone, A.; Simmonds, D.J.; D'Alessandro, F.; Frega, F. Prediction of Shoreline Evolution. Reliability of a General Model for the Mixed Beach Case. *J. Mar. Sci. Eng.* **2020**, *8*, 361. [CrossRef]
10. Roelvink, J.A.; Van Banning, G.K.F.M. Design and development of delft3d and application to coastal morphodynamics. *Oceanogr. Lit. Rev.* **1995**, *11*, 925.

11. Roelvink, D.; Reniers, A.J.H.M.; Van Dongeren, A.; Van Thiel de Vries, J.; Lescinski, J.; McCall, R. Xbeach model description and manual. *Unesco-Ihe Inst. Water Educ. Deltares Delft Univ. Technol. Rep. June* **2010**, *21*, 2010.
12. Warren, I.R.; Bach, H.K. Mike 21: A modelling system for estuaries, coastal waters and seas. *Environ. Softw.* **1992**, *7*, 229–240. [CrossRef]
13. Yates, M.L.; Guza, R.T.; O'reilly, W.C. Equilibrium shoreline response: Observations and modeling. *J. Geophys. Res. Ocean.* **2009**, *114*. [CrossRef]
14. Davidson, M.A.; Splinter, K.D.; Turner, I.L. A simple equilibrium model for predicting shoreline change. *Coast. Eng.* **2013**, *73*, 191–202. [CrossRef]
15. Kriebel, D.L.; Dean, R.G. Convolution method for time-dependent beach-profile response. *J. Waterw. Port Coast. Ocean. Eng.* **1993**, *119*, 204–226. [CrossRef]
16. Wright, L.D.; Short, A.D. Morphodynamic variability of surf zones and beaches: A synthesis. *Mar. Geol.* **1984**, *56*, 93–118. [CrossRef]
17. Schepper, R.; Almar, R.; Bergsma, E.; de Vries, S.; Reniers, A.; Davidson, M.; Splinter, K. Modelling Cross-Shore Shoreline Change on Multiple Timescales and Their Interactions. *J. Mar. Sci. Eng.* **2021**, *9*, 582. [CrossRef]
18. Pelnard-Considère R. Theoretical Tests on the Shoreline Evolution of Sand and Gravel Beaches. In Proceedings of the 4èmes Journées de l'Hydraulique, Paris, France, 13–15 June 1956; pp. 289–298.
19. Turki, I.; Medina, R.; Coco, G.; Gonzalez, M. An equilibrium model to predict shoreline rotation of pocket beaches. *Mar. Geol.* **2013**, *346*, 220–232. [CrossRef]
20. Dronkers, J. *Dynamics of Coastal Systems*; World Scientific: Singapore, 2005; Volume 25.
21. Coastal Engineering Research Center (US). *Shore Protection Manual*; Department of the Army, Waterways Experiment Station, Corps of Engineers, Coastal Engineering Research Center: Washington, DC, USA, 1984.
22. Ashton, A.; Murray, A.B.; Arnoult, O. Formation of coastline features by large-scale instabilities induced by high-angle waves. *Nature* **2001**, *414*, 296–300. [CrossRef]
23. Hurst, M.D.; Barkwith, A.; Ellis, M.A.; Thomas, C.W.; Murray, A.B. Exploring the sensitivities of crenulate bay shorelines to wave climates using a new vector-based one-line model. *J. Geophys. Res. Earth Surf.* **2015**, *120*, 2586–2608. [CrossRef]
24. Roelvink, D.; Huisman, B.; Elghandour, A.; Ghonim, M.; Reyns, J. Efficient modelling of complex sandy coastal evolution at monthly to century time scales. *Front. Mar. Sci.* **2020**, *7*, 535. [CrossRef]
25. Medellin, G.; Torres-Freyermuth, A.; Tomasicchio, G.R.; Francone, A.; Tereszkiewicz, P.A.; Lusito, L.; Palemon-Arcos, L.; Lopez, J. Field and Numerical Study of Resistance and Resilience on a Sea Breeze Dominated Beach in Yucatan (Mexico). *Water* **2018**, *10*, 1806. [CrossRef]
26. Bruun, P. Sea-level rise as a cause of shore erosion. *J. Waterw. Harb. Div.* **1962**, *88*, 117–130. [CrossRef]
27. Thuan, D.H.; Almar, R.; Marchesiello, P.; Viet, N.T. Video Sensing of Nearshore Bathymetry Evolution with Error Estimate. *J. Mar. Sci. Eng.* **2019**, *7*, 233. [CrossRef]
28. Marchesiello, P.; Kestenare, E.; Almar, R.; Boucharel, J.; Nguyen, N.M. Longshore drift produced by climate-modulated monsoons and typhoons in the South China Sea. *J. Mar. Syst.* **2020**, *211*, 103399. [CrossRef]
29. Almar, R.; Marchesiello, P.; Almeida, L.P.; Thuan, D.H.; Tanaka, H.; Viet, N.T. Shoreline response to a sequence of typhoon and monsoon events. *Water* **2017**, *9*, 364. [CrossRef]
30. Bertsimas, D.; Tsitsiklis, J. Simulated annealing. *Stat. Sci.* **1993**, *8*, 10–15 [CrossRef]
31. Thuan, D.H.; Binh, L.T.; Viet, N.T.; Hanh, D.K.; Almar, R.; Marchesiello, P. Typhoon impact and recovery from continuous video monitoring: A case study from Nha Trang Beach, Vietnam. *J. Coast. Res.* **2016**, *75*, 263–267. [CrossRef]
32. Almeida, L.P.; Almar, R.; Blenkinsopp, C.; Senechal, N.; Bergsma, E.; Floc'h, F.; Caulet, C.; Biausque, M.; Marchesiello, P.; Grandjean, P.; et al. Lidar Observations of the Swash Zone of a Low-Tide Terraced Tropical Beach under Variable Wave Conditions: The Nha Trang (Vietnam) COASTVAR Experiment. *J. Mar. Sci. Eng.* **2020**, *8*, 302. [CrossRef]
33. Andriolo, U.; Almeida, L.P.; Almar, R. Coupling terrestrial LiDAR and video imagery to perform 3D intertidal beach topography. *Coast. Eng.* **2018**, *140*, 232–239. [CrossRef]
34. Tran, H.Y. Modeling Long Term Shoreline Evolution and Coastal Erosion. Ph.D. Thesis, Université Grenoble Alpes, Grenoble, France, 2018.
35. Booij, N.R.R.C.; Ris, R.C.; Holthuijsen, L.H. A third-generation wave model for coastal regions: 1. Model description and validation. *J. Geophys. Res. Ocean.* **1999**, *104*, 7649–7666. [CrossRef]
36. Bertin, X.; Castelle, B.; Chaumillon, E.; Butel, R.; Quique, R. Longshore transport estimation and inter-annual variability at a high-energy dissipative beach: St. Trojan beach, SW Oléron Island, France. *Cont. Shelf Res.* **2008**, *28*, 1316–1332. [CrossRef]
37. Battjes, J.A. Surf similarity. In Proceedings of the 14th International Conference on Coastal Engineering, Copenhagen, Denmark, 24–28 June 1975; pp. 466–480.
38. Galvin, C.J., Jr. Breaker type classification on three laboratory beaches. *J. Geophys. Res.* **1968**, *73*, 3651–3659. [CrossRef]
39. Daly, C.; Floc'h, F.; Almeida, L.P.; Almar, R. Modelling accretion at Nha Trang Beach, Vietnam. *Icoastal Dyn.* **2017**, *170*, 1886–1896.
40. Dalya, C.J.; Floc'h, F.; Almeida, L.P.; Almara, R.; Jaud, M. Morphodynamic modelling of beach cusp formation: The role of wave forcing and sediment composition. *Geomorphology* **2021**, *389*, 107798. [CrossRef]
41. Davidson, M. Forecasting coastal evolution on time-scales of days to decades. *Coast. Eng.* **2021**, *168*, 103928. [CrossRef]
42. Bird, E.C. *Coastal Geomorphology: An Introduction*; John Wiley & Sons: Hoboken, NJ, USA, 2011.

43. Vos, K.; Harley, M.D.; Splinter, K.D.; Walker, A.; Turner, I.L. Beach Slopes from Satellite-Derived Shorelines. *Geophys. Res. Lett.* **2020**, *47*, e2020GL088365. [CrossRef]
44. Bergsma, E.W.; Almar, R. Coastal coverage of ESA'Sentinel 2 mission. *Adv. Space Res.* **2020**, *65*, 2636–2644. [CrossRef]
45. Taveneau, A.; Almar, R.; Bergsma, E.W.; Sy, B.A.; Ndour, A.; Sadio, M.; Garlan, T. Observing and Predicting Coastal Erosion at the Langue de Barbarie Sand Spit around Saint Louis (Senegal, West Africa) through Satellite-Derived Digital Elevation Model and Shoreline. *Remote Sens.* **2021**, *13*, 2454. [CrossRef]